universe

IMPACT FACTOR 2.9

CITESCORE 3.6

Article

Effective Potential for Quintessential Inflation Driven by Extrinsic Gravity

Abraão J. S. Capistrano and Luís Antonio Cabral

Special Issue
Universe: Feature Papers 2023—Cosmology

Edited by
Dr. Kazuharu Bamba

MDPI

https://doi.org/10.3390/universe9120497

universe

MDPI

Article

Effective Potential for Quintessential Inflation Driven by Extrinsic Gravity

Abraão J. S. Capistrano [1,2,*] and Luís Antonio Cabral [3]

[1] Departamento de Engenharias e Ciências Exatas, Universidade Federal do Paraná, Palotina 85950-000, PR, Brazil
[2] Applied Physics Graduation Program, Federal University of Latin-American Integration, Foz do Iguassu 85867-670, PR, Brazil
[3] Curso de Física, Setor Cimba, Universidade Federal do Norte do Tocantins, Araguaína 77824-838, TO, Brazil; cabral@mail.uft.edu.br
* Correspondence: capistrano@ufpr.br

Abstract: We numerically study the evolution of the extrinsic energy density in the context of an inflationary regime at the background level in a five-dimensional model using a Bayesian analysis from a dynamic nested sampler (`DYNESTY`) code. By means of the Nash–Greene embedding theorem, we show that the corresponding model provides an effective potential driven by the influence of extrinsic geometry. We obtain a quintessential inflation that defines a model with a potential $V(\phi) = e^{-\alpha_1\phi}(1 - \alpha_2\phi^2)$, where α_1 and α_2 are dimensionless parameters. Using some known phenomenological parameterizations, such as Chevallier–Polarski–Linder (CPL) and Barboza–Alcaniz (BA) parameterizations, we show that the model reflects a slow-varying inflation preferring a thawing behavior, suggesting an optimistic scenario for further research on the unification of inflation with late cosmic acceleration.

Keywords: inflation; Nash–Greene theorem; gravitational field

Citation: Capistrano, A.J.S.; Cabral, L.A. Effective Potential for Quintessential Inflation Driven by Extrinsic Gravity. *Universe* **2023**, *9*, 497. https://doi.org/10.3390/universe9120497

Academic Editor: Kazuharu Bamba

Received: 9 October 2023
Revised: 20 November 2023
Accepted: 25 November 2023
Published: 28 November 2023

1. Introduction

Cosmic inflation is one of the most fantastic mechanisms for understanding the evolution of the early universe, which underwent a rapid and exponential increase in the cosmic scale factor shortly after the Big Bang. It proposes a simple solution to the horizon problem by suggesting that far-reaching regions of the universe were in close proximity before inflation occurred. Then, it explains why the universe appears homogeneous and isotropic on large scales. Moreover, the so-called *flatness problem* that states, *Why does the universe seem to have a nearly flat geometry*? is solved in the context of inflation since it naturally leads to a flat universe [1]. It also provides an explanation of the formation of a large-scale structure in the universe, including galaxies and galaxy clusters, by quantum fluctuations in a peculiar scalar field dubbed as *inflaton field* during that cosmic inflationary period [2–9].

The nature of the inflaton field motivated the elaboration of a plethora of competing cosmological models [10–19] due to the fact that the form of the inflation field is not determined and the standard phenomenological model Λ cold dark matter (ΛCDM) with the fluid parameter $w = -1$ rapidly decays at the end of the inflationary period [20]. Thus, the inflaton field cannot be directly regarded as a cosmological constant Λ for the late acceleration of the universe. An immediate issue arises whether the inflaton field should be some form of a dark energy (DE) fluid: *how does the equation of the state parameter w significantly deviate from* $w = -1$ *during the inflationary era?* In this paper, we make the first steps to answer this question in the context of a modification of gravity by extra dimensions. Apart from traditional models, such as the Arkani-Hamed–Dvali–Dimopoulos (ADD) model [21], the Randall–Sundrum model [22,23], and/or the Dvali–Gabadadze–Porrati model (DPG) [24], we explore the dynamical embedding of space-times as the

main mathematical structure [25–40]. In *Encyclopaedia Inflationaris* [41], the reader can find various types and classifications of inflationary models, such as supergravity brane inflation, supersymmetry (SUSY), and brane inflation models.

The paper is organized into sections. The second and third sections summarize the essentials of previously published results on the construction of the four-dimensional embedded model and cosmological applications [26–28,31,39,40]. The fourth section presents the fluid analogy necessary to make a comparison with phenomenological models. Moreover, we construct a model wherein the extrinsic curvature is thought as an inflaton field as shown in the fifth section. By means of numerical analysis generating synthetic random points using the `DYNESTY` [42,43] Python code, we constrain the parameters of our toy model. To analyze how the related equation of state (EoS) evolves, we use Chevallier–Polarski–Linder (CPL) [44,45] and Barboza–Alcaniz (BA) [46] parameterizations to distinguish the present model as a *thawing* [47–49] or *freezing* [50–53] pattern. Thawing models are conceived to be those that the fluid parameter as a function of the redshift $w(z)$ in EoS is moving away from -1, which means that DE density decreases over time, gradually allowing the universe to accelerate more rapidly. On the other hand, in freezing models, DE density remains approximately constant as the universe expands, with $w(z)$ approaching the value -1. Finally, the conclusion and prospects are presented in the *Remarks* section.

2. Essentials on Embeddings

We define a model endowed with a gravitational action S in the presence of confined matter fields wherein a four-dimensional embedded space-time is embedded in five dimensions as

$$S = -\frac{1}{2\kappa_5^2}\int \sqrt{|\mathcal{G}|}\left({}^5\mathcal{R} + \mathcal{L}_m^*\right)d^5x\,, \tag{1}$$

where κ_5^2 is a fundamental energy scale on the embedded space, and the curly ${}^5\mathcal{R}$ denotes the five-dimensional Ricci scalar of the bulk given by the summation of the four-dimensional Ricci scalar R and the deformation scalar Q and has the simple form ${}^5\mathcal{R} = R + Q$. Moreover, $\mathcal{L}_m^*$ denotes the bulk source Lagrangian in five dimensions. Since gravity should only propagate in the bulk, $\mathcal{L}_m^*$ is localized in the four-dimensional embedded space and obeys the confinement condition

$$\begin{aligned} \kappa_5^2 T^*_{\mu\nu} &= -8\pi G T_{\mu\nu}\,, \\ \kappa_5^2 T^*_{\mu a} &= 0\,, \\ \kappa_5^2 T^*_{ab} &= 0\,, \end{aligned} \tag{2}$$

from the components of $\mathcal{T}_{AB}$ of the energy–momentum tensor of the bulk. The terms of $T^*_{\mu\nu}$, $T^*_{\mu a}$, and T^*_{ab} denote the energy–momentum of the tangent (tensor), vector, and scalar components of $\mathcal{T}_{AB}$. Concerning notation, capital Latin indices are fixed to 5 to reinforce the notation of a five-dimensional space. Small-case Latin indices refer to the only one extra dimension fixed to 1. All Greek indices refer to the embedded space-time running from 1 to 4. Ordinary matter and gauge fields are represented by $T_{\mu\nu}$, and G is the gravitational Newtonian constant. From the set of equations in Equation (2), $\mathcal{L}_m^*$ reduces to the confined four-dimensional Lagrangian $\mathcal{L}_m$ related to $T_{\mu\nu}$ as

$$T_{\mu\nu} = -\frac{2}{\sqrt{|g|}}\frac{\delta\left(\sqrt{|g|}\mathcal{L}_m\right)}{\delta\, g^{\mu\nu}}\,, \tag{3}$$

where $g_{\mu\nu}$ is the metric and $|g|$ is the absolute value of $g_{\mu\nu}$. Detailed demonstrations of the fundamental field equations, from a bulk of five or in arbitrary dimensions, can be found in Refs. [26–28,31,40]. In this work, in search of constructing a viable physical model, we consider the extrinsic curvature as a main character of cosmic dynamics. Mathematically speaking, besides the metric $g_{\mu\nu}$, such new curvature is a pivotal element in the embedding

of geometries. As traditionally defined in [54], the nonperturbed extrinsic curvature $k_{\mu\nu}$ reads,

$$k_{\mu\nu} = -\mathcal{X}^{A}_{,\mu}\, \eta^{B}_{,\nu} \mathcal{G}_{AB}\,. \tag{4}$$

The definition in Equation (4) essentially means a measure of *bending* of the embedded geometry; i.e., it reflects how a normal unitary vector η^A in the embedded space deviates from the tangent plane. Let the coordinate $\mathcal{X}$ define a regular map $\mathcal{X} : V_4 \to V_5$. Such a local map states that a Riemannian manifold V_4 is isometrically embedded in a larger five-dimensional Riemannian bulk space V_5. The term $\mathcal{G}_{AB}$ is the bulk metric

$$\mathcal{G}_{AB} \;=\; \begin{pmatrix} g_{\mu\nu} & 0 \\ 0 & 1 \end{pmatrix}. \tag{5}$$

Another pivotal relation is Nash's deformation formula given by

$$k_{\mu\nu} = -\frac{1}{2}\frac{\partial g_{\mu\nu}}{\partial y}\,, \tag{6}$$

where y is an arbitrary spatial coordinate. Nash's deformation formula is the pivot result of Nash's embedding theorem of 1954 applied to non-Euclidean metrics [55]. In 1956, Nash generalized his former results to Riemannian metrics [56]. Decades later, Nash's theorem was expanded to non-Riemannian metrics by Greene [57]. From a physical point of view, Equation (6) localizes gravity closer to the four-dimensional embedded space, imposing a strong bending (warping) geometrical constraint.

Nash's results in Equation (6) is the capital element to obtain a solution to well-known Gauss and Codazzi equations given by

$$^{5}\mathcal{R}_{ABCD}\mathcal{Z}^{A}{}_{,\alpha}\mathcal{Z}^{B}{}_{,\beta}\mathcal{Z}^{C}{}_{,\gamma}\mathcal{Z}^{D}{}_{,\delta} = R_{\alpha\beta\gamma\delta} + \left(k_{\alpha\gamma}\, k_{\beta\delta} - k_{\alpha\delta}\, k_{\beta\gamma}\right), \tag{7}$$

$$^{5}\mathcal{R}_{ABCD}\mathcal{Z}^{A}{}_{,\alpha}\mathcal{Z}^{B}{}_{,\beta}\mathcal{Z}^{C}{}_{,\gamma}\eta^{D} = k_{\alpha[\beta;\gamma]}\,, \tag{8}$$

where $^{5}\mathcal{R}_{ABCD}$ denotes the five-dimensional Riemann tensor, and $R_{\alpha\beta\gamma\delta}$ is the four-dimensional Riemann tensor. The coordinate $\mathcal{Z}^{A}_{,\mu}$ is a perturbed coordinate in the sense that $\mathcal{Z}^{A}_{,\mu} = \mathcal{X}^{A}_{,\mu} + \delta y\, \eta^{A}_{,\mu}$. The semicolon sign in Equation (8) represents the ordinary covariant derivative with respect to the metric $g_{\mu\nu}$ and $k_{\alpha[\beta;\gamma]} \equiv k_{\alpha\beta;\gamma} - k_{\alpha\gamma;\beta}$. The importance of Equations (7) and (8) is that they reflect the integrability conditions for the embedding explicitly relating the bulk and embedded space, and they are the starting point to obtain the induced field equations [26–28,31,40].

3. Friedmann–Lemaître–Robertson–Walker (FLRW) Embedded Cosmology

From integration of Equations (7) and (8), one obtains the induced four-dimensional nonperturbed field equations as

$$G_{\mu\nu} - Q_{\mu\nu} \;=\; -8\pi G T_{\mu\nu}\,, \tag{9}$$

$$k_{\mu[\nu;\rho]} \;=\; 0\,, \tag{10}$$

where $T_{\mu\nu}$ is the energy–momentum tensor of the confined sources, G is the gravitational Newtonian constant, and $G_{\mu\nu}$ is the four-dimensional Einstein tensor. The deformation tensor $Q_{\mu\nu}$ is given by

$$Q_{\mu\nu} = k^{\rho}_{\mu}k_{\rho\nu} - k_{\mu\nu}h - \frac{1}{2}\left(K^2 - h^2\right)g_{\mu\nu}\,, \tag{11}$$

where the mean curvature is given by $h^2 = h{\cdot}h$ and $h = \; g^{\mu\nu}\, k_{\mu\nu}$. The quantity $K^2 = k^{\mu\nu}k_{\mu\nu}$ is the Gaussian curvature. By direct derivation, Equation (11) is conserved in the sense that

$$Q_{\mu\nu;\mu} = 0\,. \tag{12}$$

Once the field equations of Equations (9) and (10) are set, we obtain the background cosmic evolution from the usual four-dimensional line element of the FLRW metric given by

$$ds^2 = a^2\left(dr^2 + r^2 d\theta^2 + r^2 \sin^2\theta d\phi^2\right) - dt^2 \,, \tag{13}$$

where $a \equiv a(t)$ is the scale factor and t is the physical time. As shown in previous works [27,31], the solutions of Equations (9) and (10) are summarized as

$$k_{ij} = \frac{b}{a^2} g_{ij} \ (i,j = 1,2,3) \,, \tag{14}$$

$$k_{44} = \frac{-1}{\dot{a}} \frac{d}{dt} \frac{b}{a} \,, \tag{15}$$

$$k_{44} = -\frac{b}{a^2}\left(\frac{B}{H} - 1\right) \,, \tag{16}$$

$$K^2 = \frac{b^2}{a^4}\left(\frac{B^2}{H^2} - 2\frac{B}{H} + 4\right), \ h = \frac{b}{a^2}\left(\frac{B}{H} + 2\right), \tag{17}$$

$$Q_{ij} = \frac{b^2}{a^4}\left(2\frac{B}{H} - 1\right) g_{ij}, \ Q_{44} = -\frac{3b^2}{a^4}, \tag{18}$$

$$Q = -(K^2 - h^2) = \frac{6b^2}{a^4}\frac{B}{H} \,, \tag{19}$$

where Q is the deformation scalar given by the contraction $g^{\mu\nu}Q_{\mu\nu} = Q$, and $H \equiv H(t) = \frac{\dot{a}}{a}$ is the Hubble parameter. Defined as an "extrinsic" copy of the Hubble parameter H, we have the cosmic bending parameter $B = B(t) \equiv \frac{\dot{b}}{b}$. The obtainment of these results is shown in detail in Refs. [27,31]. The *warping* or *bending* function $b(t)$ is given by

$$b(t) = \frac{b_0}{a_0^{\beta_0}} a(t)^{\beta_0} \,, \tag{20}$$

where the parameter b_0 denotes the current value of $b(t)$ and a_0 is the current value of the scale factor.

4. The Fluid Analogy

We obtain the hydrodynamical equations for a perfect fluid in comoving coordinates as the same way as in the usual general relativity (GR) framework. Thus, the stress energy tensor $T_{\mu\nu}$ has the standard form

$$T_{\mu\nu} = (\rho + p) u_\mu u_\nu + p g_{\mu\nu} \ ; \ u_\mu = \delta^4_\mu \,, \tag{21}$$

and the conservation equation

$$\rho + 3H(\rho + p) = 0 \,, \tag{22}$$

from $T_{\mu\nu;\mu} = 0$. Hence, one obtains the resulting Friedmann equation as

$$H^2 = \frac{8}{3}\pi G\rho + \frac{b^2}{a^4} \,, \tag{23}$$

where $\rho \equiv \rho_m(t)$ is the nonperturbed matter density. Using Equations (20) and (23), we have

$$H^2 = \frac{8}{3}\pi G\rho_{m(0)} a^{-3} + \frac{b_0^2}{a_0^{2\beta_0}} a^{2\beta_0 - 4} \,, \tag{24}$$

where $\rho_{m(0)}$ is the current value of matter energy density. With respect to the cosmological parameters $\Omega_{\mathbf{i}} = \frac{8\pi G}{3H_0^2}\rho_{i(0)}$, $\mathbf{i}$ identifies the density species, and considering only *matter* and *extrinsic* species, we write the Hubble evolution $H(z)$ simply as

$$H(z) = H_0\sqrt{\Omega_m(z) + \Omega_{ext}(z)}\,, \tag{25}$$

where $H(z)$ is the Hubble parameter in terms of the redshift $z = \frac{1-a}{a}$. The matter density parameter is denoted by $\Omega_m(z) = \Omega_{m(0)}(1+z)^3$. The term $\Omega_{ext}(z) = \Omega_{ext(0)}(1+z)^{4-2\beta_0}$ stands for the density parameter associated with the extrinsic curvature. The cosmological parameters $\Omega_{m(0)}$ and $\Omega_{ext(0)} = b_0^2/H_0^2 a_0^{2\beta_0}$ denote the present value of the matter and extrinsic contributions, respectively. The current warp (bending) of the universe denoted by b_0 has the same dimension as H_0 that is the current value of a Hubble constant in units of km·s^{-1} Mpc^{-1}. If $\Omega_{ext}(z)$ vanishes with $b_0 \to 0$, one obtains GR limit as a background with the recovery of Einstein equations. For a flat universe, we have $\Omega_{ext(0)} = 1 - \Omega_{m(0)}$.

To obtain an effective cosmological model in order to make tests with real data, an effective "extrinsic fluid parameter" w_{ext} must be set. We define a "fluid analogy" by means of an effective equation of state (EoS) as

$$w_{ext} = -1 + \frac{1}{3}(4 - 2\beta_0)\,, \tag{26}$$

in which the equality $w_{ext} = w$ happens if $\beta_0 = \frac{1}{2}(1-3w)$, where the dimensionless fluid parameter w defines an EoS related to pressure p and energy density ρ as $w = \frac{p}{\rho}$. Thus, one defines the dimensionless Hubble parameter $E(z) \equiv \frac{H}{H_0}$ that reads

$$E^2(z) = \Omega_{m(0)}(1+z)^3 + \Omega_{ext(0)}(1+z)^{3(1+w)}\,, \tag{27}$$

which resembles an XCDM fluid [58].

5. Extrinsic Curvature as an Effective Inflaton Field

Besides Equations (26) and (27), we can explore the effective fluid approach rewriting Equation (9) in the form

$$R_{\mu\nu} - \frac{1}{2}R\bar{g}_{\mu\nu} = -8\pi G\bar{T}_{total}\,, \tag{28}$$

where $\bar{T}^{total}_{\mu\nu} = \bar{T}_{\mu\nu} + \frac{1}{8\pi G}\bar{T}^{ext}_{\mu\nu}$. The quantity $\bar{T}^{ext}_{\mu\nu} \doteq Q_{\mu\nu}$ denotes the extrinsic contribution. Mimicking Equation (21), we write $\bar{T}^{ext}_{\mu\nu}$ as

$$\bar{T}^{ext}_{\mu\nu} = (\bar{p}_{ext} + \bar{\rho}_{ext})u_\mu u_\nu + \bar{p}_{ext}\,\bar{g}_{\mu\nu}, \quad u_\mu = \delta^4_\mu\,, \tag{29}$$

where u_μ is the comoving four velocities. It is worth noting that the deformation tensor $Q_{\mu\nu}$ is independently conserved as shown in Equation (12), so is $\bar{T}^{ext}_{\mu\nu}$. We stress that the dynamical embedding naturally warrants the influence of the bulk over the embedded space, such as quantities $Q_{\mu\nu}$ with a mixture of intrinsic and extrinsic terms, as shown in Equation (11). As a consequence, $\bar{T}^{ext}$ is conserved unless an exotic matter-energy source is added. This result differs from a DE fluid in standard rigid brane-world models [22–24], where $\bar{T}^{ext}$ is not conserved due to the necessity of the bulk–brane energy exchange.

From the conservation of Equation (29), we obtain

$$\frac{d\bar{\rho}_{ext}}{dt} + 3H(\bar{\rho}_{ext} + \bar{p}_{ext}) = 0\,. \tag{30}$$

In a perfect fluid analogy with Equation (22), $\bar{\rho}_{ext}$ denotes the nonperturbed "extrinsic" energy density given by

$$\bar{\rho}_{ext}(a) = \rho_{ext(0)}a^{-3(1+w)}\,, \tag{31}$$

where the current "extrinsic" energy density is $\rho_{ext(0)} = \frac{3b_0^2}{8\pi G a_0^{1-3w}}$. Therefore, the "extrinsic" pressure $\bar{p}_{ext}$ is straightforwardly calculated by Equation (30) to obtain

$$\bar{p}_{ext}(a) = w\rho_{ext(0)}a^{-3(1+w)} \, . \tag{32}$$

When $b_0 \to 0$, the extrinsic curvature ceases, and $\bar{T}^{ext}_{\mu\nu}$, $\bar{\rho}_{ext}(a)$, and $\bar{p}_{ext}(a)$ vanish, and the GR limit is reached. Alternatively, one writes the related Friedman equation in the form

$$H^2 = \frac{8}{3}\pi G(\bar{\rho}_m + \bar{\rho}_{ext}) \, . \tag{33}$$

5.1. The Extrinsic Inflaton Field

Since $\bar{\rho}_{ext}$ plays a role in driving the late accelerated expansion as explored in [27,31], the same energy density $\bar{\rho}_{ext}$ should have the dynamics of a scalar field potential energy density $V(\phi)$ during early inflationary periods generated by the "extrinsic scalar" field ϕ. Hence, the related Lagrangian $\mathcal{L}_\phi$ is defined as

$$\mathcal{L}_\phi = \frac{1}{2}\dot{\phi}^2 - V(\phi) \, . \tag{34}$$

The form written in Equation (34) shows that the field ϕ is spatially homogeneous; then it only depends on the cosmic time t. In addition, the related energy momentum of such a field is written as

$$T^{\phi}_{\mu\nu} = \partial_\mu\phi \, \partial_\nu\phi + g_{\mu\nu}\left(\frac{1}{2}\dot{\phi}^2 - V(\phi)\right) \, . \tag{35}$$

From the conservation of Equation (35), i.e., $T^{\phi}_{\mu\nu;\mu} = 0$, one obtains the correspondence relations

$$\bar{\rho}_{ext} = \bar{\rho}_\phi = \frac{\dot{\phi}^2}{2} + V(\phi) \, , \tag{36}$$

$$\bar{p}_{ext} = \bar{p}_\phi = \frac{\dot{\phi}^2}{2} - V(\phi) \, , \tag{37}$$

where the dot symbol denotes an ordinary derivative with respect to the cosmic time t. The forms of Equations (36) and (37) couple with the inflation dynamics given by $V(\phi)$ to the background evolution. Then, the quantities $\bar{\rho}_{ext}$ and $\bar{p}_{ext}$ can be written as a function of the extrinsic scalar field ϕ.

In terms of fluid analogy given by Equation (26) and the direct sum of Equations (36) and (37), and using Equations (31) and (32), one obtains

$$\dot{\phi}(a) = \sqrt{\rho_{ext(0)}(1+w)}a^{-\frac{3}{2}(1+w)} \, . \tag{38}$$

Using the relation $\dot{\phi} = aH\frac{\phi}{da}$ and the inflation condition $H^2(a) \sim \frac{8\pi G}{3}\rho_{ext}(a)$, we integrate Equation (38) to obtain the potential $\phi(a)$ as

$$\phi(a) = \sqrt{|\frac{3(1+w)}{8\pi}|} \, M_{pl} \ln a \, , \tag{39}$$

where we denote the Planck mass as $M_{pl} = \frac{1}{\sqrt{G}}$. We consider the initial conditions $\phi_{ini} = 0$ and $a_{ini} = 1$. Putting the solution of Equation (39) in Equation (36), one obtains a potential $V(\phi)$ in the form

$$V(\phi) = V_0 e^{-\alpha_0\phi/M_{pl}} \, . \tag{40}$$

For the sake of notation, we denote the quantity α_0 in Equation (40) as $\alpha_0 = \sqrt{|24\pi(1+w)|}$. The models of such exponential form produce a *power law inflation* (PLI), first introduced in Refs. [59–61]. For the time being, this type of potential has strong constraints imposed

by Planck data [62] and is ruled out at more than 2-σ confidence regions. Moreover, PLI inflation requires a *graceful exit* in the slow-roll approximation. In such a model, the first slow-roll Hubble parameter is constant that leads to an eternal inflation [41]. Such potential was also studied in the context of M-theory [63] and RSII scenarios [64]. Due to the strong constraints on PLI, based on Equation (40), our numerical study will take an effective quintessential dimensionless potential $V(\phi)_{eff}$ to generalize Equation (40), such as

$$V(\phi)_{eff} = V_{PLI}(\phi) + V_{LMI}(\phi) \, , \tag{41}$$

where $V_{PLI}(\phi)$ denotes our PLI potential given by Equation (40). The quantity $V_{LMI}(\phi)$ denotes a phenomenological potential that defines the so-called *logamediate inflation* (LMI) [65,66] in the form

$$V_{LMI}(\phi) = V_0 \, \gamma_3 \left(\frac{\phi}{M_{pl}} \right)^{\gamma_2} e^{-\gamma_1 \left(\frac{\phi}{M_{pl}} \right)^{\gamma_4}} \, , \tag{42}$$

in which $(\gamma_1, \gamma_2, \gamma_3, \gamma_4)$ are free dimensionless parameters. For our purposes, we need to impose on Equation (40) $V_0 = \tilde{V}_0 = 1$, $\alpha_0 = \alpha_1$, and $\phi = \tilde{\phi} M_{pl}$. A similar adaptation is applied to Equation (42) with $V_0 = \tilde{V}_0 = 1$, $\gamma_1 = \alpha_1$, $\gamma_2 = 2$, $\gamma_3 = -|\alpha_2|$ $(\alpha_2 > 0)$, $\gamma_4 = 1$, and $\phi = \tilde{\phi} M_{pl}$. Hence, the resulting potential $V(\phi)_{eff}$ is given by

$$V(\phi)_{eff} = \tilde{V}_0 \, e^{-\alpha_1 \tilde{\phi}} (1 - \alpha_2 \tilde{\phi}^2) \, . \tag{43}$$

We point out that (α_1, α_2) are dimensionless parameters. Assuming that the field should roll in a direction wherein $\frac{\partial V(\phi)_{eff}}{\partial \phi} = 0$, starting at $\phi = \phi_{\min} = 1$, one obtains the condition $\alpha_2 = |\frac{\alpha_1}{2 - \alpha_1}| > 0$. For our purposes, the positivity of α_2 warrants a logistic equation set in the domain of real numbers. Therefore, the model turns again as being a one-parameter model from an extrinsic origin. This guarantees a reheating phase without relying on any approximation in a future work. It is worth noting that when an extrinsic curvature vanishes $\alpha_1 = \alpha_0 = 0$, then $\alpha_2 = 0$, and inflation ceases.

To study the evolution of the effective fluid parameter w and the characteristics of the potential $V(\phi)_{eff}$, we adopt a dynamical system approach as in the works of Clemson and Liddle [67] and Pantazis, Nesseris, and Perivolaropoulos [68]. In the latter, they use a quintessence potential of the form

$$V(\phi) = e^{-\beta_1 \phi} (1 + \beta_2 \phi) \, , \tag{44}$$

where β_1 and β_2 are free dimensionless parameters with $\beta_1 > \beta_2$. For comparison purposes, such potential will be also taken into account as a reference in contrast with Equation (43).

5.2. Numerical Parameter Estimation

In order to obtain the parameter estimation of our toy model by the potential in Equation (43), we define a "true" model that produces a close curve pattern with the adopted priors to the reference model in Equation (44).

As shown in Figure 1, we have a comparison between the potentials from Equation (44) (blue line) and our model defined by Equation (43) (black line). They present a similar pattern with the same peak height, and the latter model presents a narrower basis of its curve (black line). Both cases positively respond to a remote future passing through an accelerated phase.

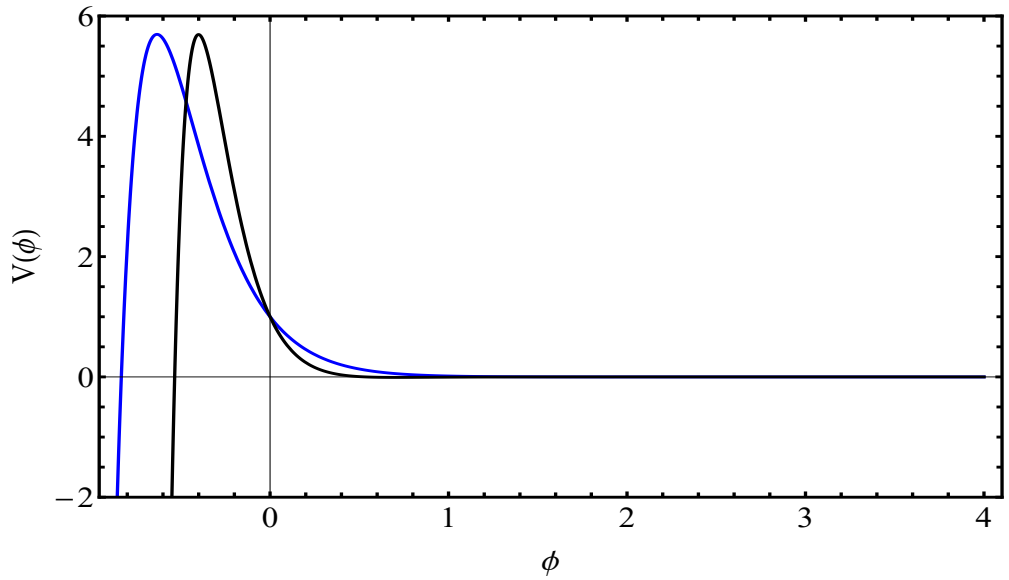

Figure 1. Comparison between the potentials from Equation (44) (blue line) and Equation (43) (black line) that indicates a close overall pattern of such potentials. The blue line was produced by adopted parameters $\{(\beta_1, \beta_2) = (5, 1.2)\}$, as shown in Ref. [68]. The black line was produced by the adopted priors that define our "true" model with the values $\{(\alpha_1, \alpha_2) = (4, 2)\}$.

In order to use the `DYNESTY` [42,43] Python code for estimating Bayesian posteriors and evidences, we adopt priors for the "true model" set as $\{(\alpha_{1(true)}, \alpha_{2(true)}, f_{(true)} = (4, 2, 1.7)\}$, where the quantity f is defined as a mechanism to control the variance in the resulting Gaussian distributions. To estimate the values of the parameters α_1 and α_2 on how they can approximate to the "true" values, we define a prior transform $u_\theta = (u_{af1}, u_{af2}, u_f)$ as

$$\alpha_1 = 5u_{af1} + 0.5; \quad (45)$$

$$\alpha_2 = 2.5u_{af2} + 0.5; \quad (46)$$

$$\ln f = 2.8u_f - 1. \quad (47)$$

We start generating n = 30000 synthetic random points and 8000 live points for better efficiency. On the other hand, under the circumstances we have defined, during the runs, we noted that generating larger random points does not change the results. To estimate both evidence and posteriors, `DYNESTY` dynamically allocates points in the runs. Each point also carries information of their covariances. It allows for creating a variable number of K_i live points at each iteration i to realize a change in a prior volume X_i. From `Numpy` 5000 random seeds and the `celerite` [69] library for a scalable Gaussian process, we obtained a total of 144659 interactions in the final of the runs. We have that the prior volume and evidence are controlled when the variation $\Delta \ln X_i \approx K_i$, as shown in Figure 2.

In Figure 3, we show the posteriors in the contour plots with the values of the parameters (α_1, α_2, f). In the lower panels, we have confidence regions for marginalized posteriors. In the upper panels, the estimated values of the parameters and their Gaussian distributions are shown. In both panels, the vertical lines indicate the values of the "true" model, defined by the priors, and horizontal lines indicate the estimated values for the model parameters.

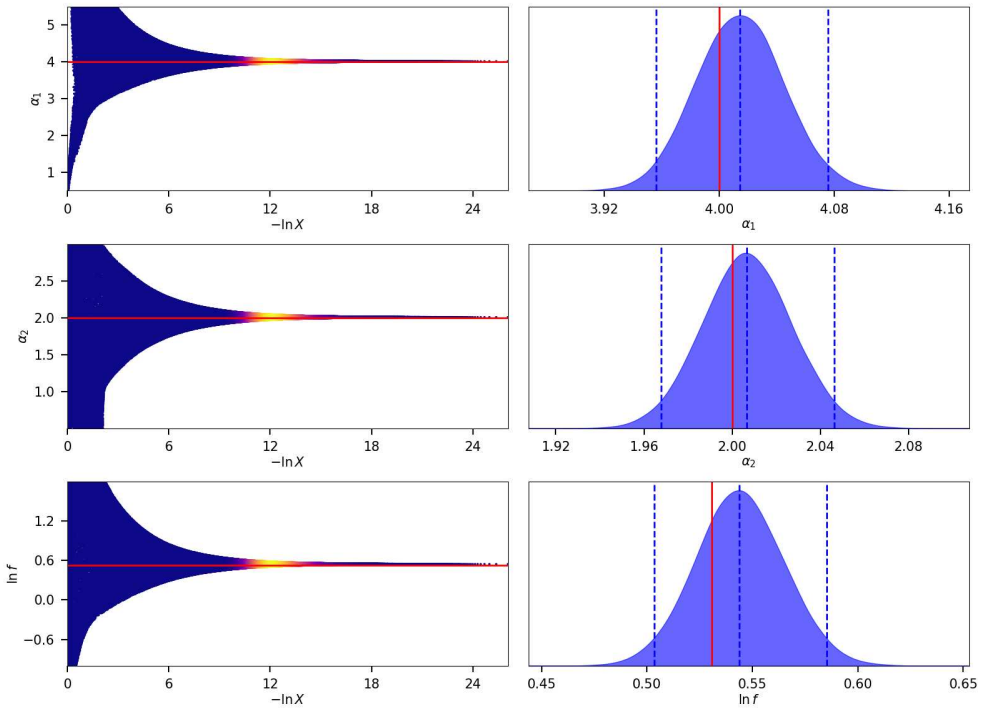

Figure 2. In the left panels, we have the control of the prior volume $\ln X_i$ of random points that shrinks exponentially over time to determine the evidence. The right panels show the posteriors (Gaussian distribution of the parameters). In both sets of panels, the red lines denote the priors ("true" values) adopted in the code.

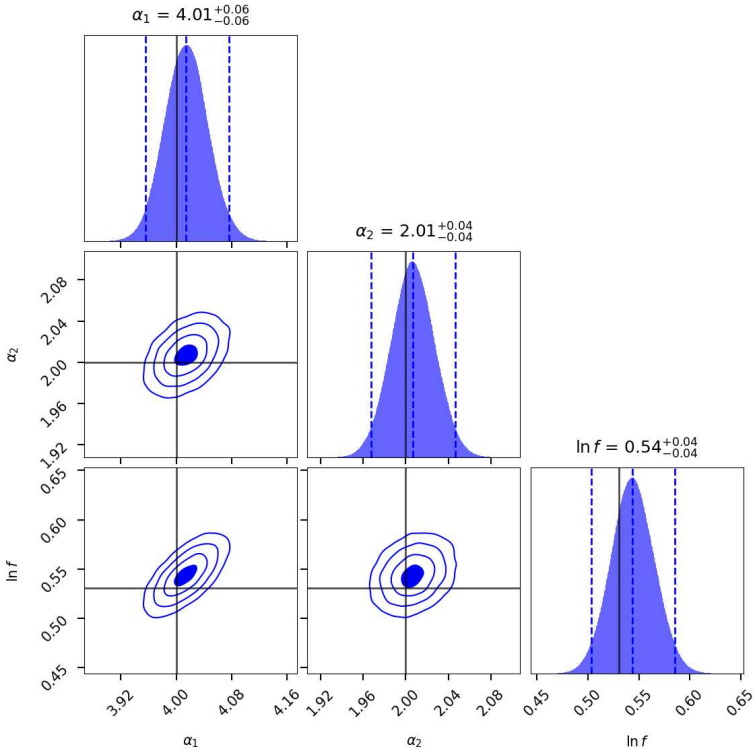

Figure 3. Contour plot for the marginalized posteriors for $(\alpha_1, \alpha_2, \ln f)$ parameters at 10%, 40%, 65%, and 85% confidence levels. Vertical dashed lines mark the 2σ region, while horizontal lines indicate the mean values of the marginalized parameters.

Using the logarithmic Jeffrey's scale [70] to input a qualitative classification of the evidence, our results indicate *barely worth-mentioning* evidence against the model as compared with the "true" model with roughly $X \sim 10^{-7}$ for the Bayes factor that is well accommodated in the range $0 \leq X < 1.1$. As traditionally known, Jeffrey's scale classifies it as weak evidence against the model with the interval $1.1 \leq X < 3$. The range $3 \leq X < 5$ indicates strong evidence disfavoring the competing model. Finally, very strong evidence against the competing model is achieved at $X \geq 5$.

5.3. Dynamical System and Comparison with the Potentials

Following Refs. [67,68], one constructs a dynamical system with the coordinates

$$x = \frac{\dot{\phi}}{\sqrt{6}H} \,, \tag{48}$$

$$y = \sqrt{\frac{V}{3H^2}} \,, \tag{49}$$

$$\lambda = \frac{-V'}{V} \,, \tag{50}$$

where the prime sign $(')$ indicates an ordinary derivative with respect to the scalar field ϕ. The variables (x, y, λ) can be written in the form of an autonomous system as

$$\frac{dx}{dN} = -3x + \sqrt{\frac{3}{2}}\lambda y^2 + \frac{3}{2}x(1 + x^2 - y^2) \,, \tag{51}$$

$$\frac{dy}{dN} = -\sqrt{\frac{3}{2}}\lambda xy + \frac{3}{2}y(1 + x^2 - y^2) \,, \tag{52}$$

$$\frac{d\lambda}{dN} = -\sqrt{6}\lambda^2(\Gamma - 1)x \,. \tag{53}$$

The quantity N is the number of e-foldings of inflation that is commonly defined as the logarithm of the scale factor $a(t)$ such as $N = N_0 + \ln a$. The term N_0 denotes the number of the e-folds set by the current time. The quantity Γ is defined in terms of the related potential as

$$\Gamma = \frac{VV''}{V'^2} \,, \tag{54}$$

in which the double prime symbol $('')$ denotes an ordinary second derivative with respect to the scalar field ϕ. From Equation (36), and using Equations (48) and (49), one obtains

$$\Omega_{ext}(x, y) = x^2 + y^2 \,, \tag{55}$$

for a locally universe flat space curvature. Defining a corresponding effective equation of the state γ_{ext}, one writes

$$\gamma_{ext} = 1 + w = \frac{2x^2}{x^2 + y^2} \,. \tag{56}$$

By direct calculations of Equations (48)–(50), with the initial value of $\lambda_{ini} = \alpha_1$, we obtain the logistic equation

$$\frac{d\lambda}{dN} = 2\sqrt{6}(\lambda - (\sqrt{\alpha_2} + \alpha_1))^2 x \,. \tag{57}$$

In Figure 4, we show the resulting curves from the models of Equation (44) (black lines) and our model defined by Equation (43) (red lines), showing the evolution for the dynamical variable λ_i running from 0.1 to 1, denoted by the outer and inner curves, respectively. The curves were obtained, setting the values of $\Omega_{ext} = \Omega_\phi = 0.68$ and the thawing initial conditions to both models as $N_0 = -15, x_i = 10^{-5}, y_i = 10^{-3}$. As a result, the evolution of the curves of our model begins earlier than the reference model in Equation (44) shown by

the red lines. In both cases, the semicircles reach the x-axis at ∼0.82. The curves close to this value are compatible with the models of late cosmic acceleration of the universe. The origin represents an initial point in an early matter domination universe.

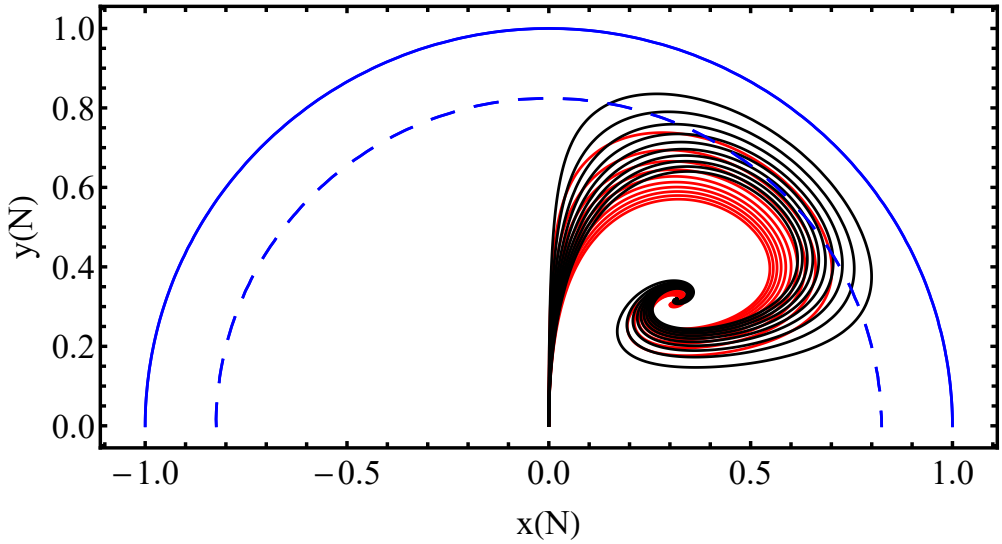

Figure 4. Comparison between the potentials from Equation (44) (black lines) and Equation (43) (red lines) that shows the evolution of the related autonomous systems. The outer continuous blue line and the dashed blue line semicircles represent the x-axis with $x \sim \sqrt{\Omega_{ext}} \sim 0.82$ and $\Omega_{ext} = \Omega_{\phi} = 0.68$, respectively.

Henceforth, we use the estimated values of the parameters of out model to evaluate how a resulting EoS of an effective $w(z)$ evolves. For this matter, we adapt the publicly code provided in [68]. The set of equations of Equations (48)–(50) has the initial conditions $N_0 = -15, x_i = 10^{-5}; y_i = 10^{-3}, \lambda[N_0] = \alpha_1$ for thawing models. For freezing models, one defines $N_0 = Log[10^{-6}], x_i = -0.5; y_i = 0.1, \lambda[N_0] = 0.1$. We use CPL parameterization as a function of the redshift written as

$$w(z) = w_0 + w_a \frac{z}{1+z}\,, \tag{58}$$

where (w_0, w_a) are parameters used to evaluate how $w(z)$ tends to depart away or converge to ΛCDM values. In conjunction with CPL, we use BA parameterization, which is given by

$$w(z) = w_0 + w_a \frac{z(1+z)}{1+z^2}\,. \tag{59}$$

We adopt the maximum value for the redshift as $z_{max} = 2$ and the maximum number of iterations i as $i_{max} = 50$.

In Figure 5, we have comparisons between CPL and BA parameterizations of the effective model in Equation (43) (with the values of Figure 5). Thus, we have a test adopting generic thawing and freezing models by means of Equations (48)–(50), and we obtain similar results as in Ref. [68]. The model prefers a thawing behavior from CPL (blue line) and BA (red line) parameterizations that are closer to numerical points (dotted line). When plotting the freezing pattern for the model, we obtained curves out of range with a large difference from the numerical curve, and they were omitted.

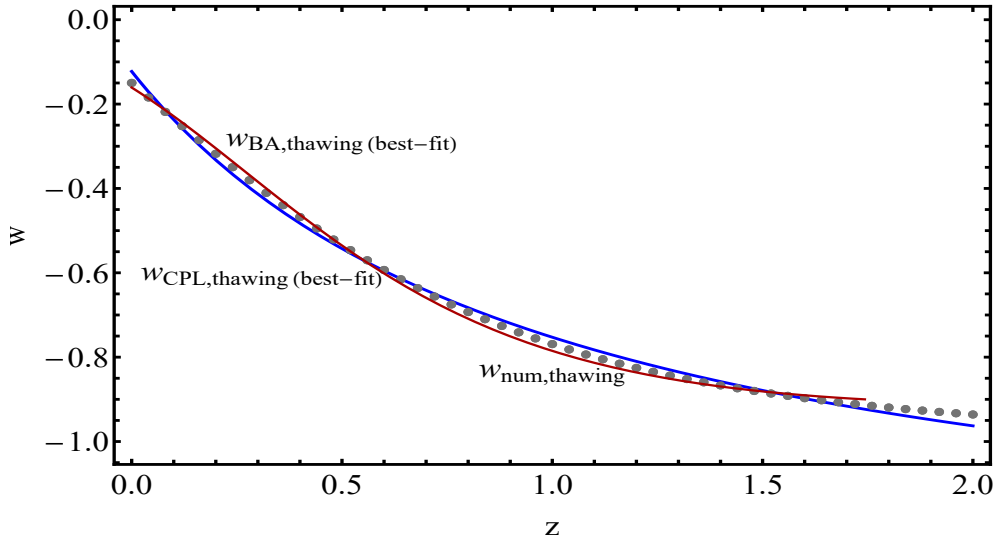

Figure 5. Behavior of numerical curves (dotted line) produced from the related autonomous system of the model preferring a thawing pattern of CPL (blue line) and BA (red line) parameterizations.

6. Remarks

We investigate the extrinsic curvature as an inflaton scalar field. The starting point lies in the correlation of the model parameter that is constrained for both accelerated regimes. For instance, the dark energy accelerated regime relies on $w < -1/3$; then we expect $w > -1/3$ for inflationary regimes in accordance with Figure 5. We also present a fluid approach in order to provide a better understanding of the related dynamics with a relation between the model parameter β_0 and the fluid parameter w, as shown in Equation (26). Our intent is to construct the basis of a geometrical model that fully relies on gravitational interactions. In this paper, we focus our attention on the inflationary period obtaining a logarithm inflaton field that generates an exponential potential in Equation (40). This form of potential creates a PLI mechanism that has strong constraints imposed by Planck data [62]. Then, we have proposed an effective form for a new potential defined in Equation (43) to generalize Equation (40). We have numerically restrained our model parameters by means of a Bayesian analysis obtained from random points using the `DYNESTY` code. Establishing a quintessential potential from a reference model of Equation (44) used in Ref. [68], we have obtained the related autonomous system of equations for forecasting models compatible with the universe evolution. Moreover, we have shown a comparison with CPL and BA parameterizations of our model that prefers a thawing cosmic scenario.

In this paper, we have considered all the cosmic components to be immutable. The numerical analysis gave us an optimistic scenario for further studies on the unification of inflation with late cosmic acceleration. The stability of the present model in this numerical evaluation allows us to use more realistic contexts to produce red spectra with a scalar spectral tilt and a small tensor-to-scalar ratio. As a subject of a future work, we will consider the full perturbation equations of the model in a scenario with a matter-sourced anisotropic stress and a series of latest astronomical data from cosmic microwave background radiation (CMB) experiments, such as Planck collaboration.

Author Contributions: Conceptualization, A.J.S.C.; formal analysis, L.A.C.; methodology, A.J.S.C. and L.A.C.; software, A.J.S.C.; supervision, L.A.C.; writing—original draft, A.J.S.C.; writing—review and editing, A.J.S.C. and L.A.C. All authors have read and agreed to the published version of the manuscript.

Funding: A.J.S.C. acknowledges Conselho Nacional de Desenvolvimento Científico e Tecnologico (CNPq, National Council for Scientific and Technological Development) for the partial financial support for this work (Grant No. 305881/2022-1) and Fundação da Universidade Federal do Paraná (FUNPAR, Paraná Federal University Foundation) through public notice 04/2023-Pesquisa/PRPPG/UFPR for the partial financial support (Process No. 23075.019406/2023-92).

Data Availability Statement: All data/codes used in this work are publicly available, and correctly cited in the references.

Acknowledgments: The authors thank the referees for their useful comments and criticisms, which substantially improved this paper.

Conflicts of Interest: The authors declare no conflict of interest.

References

1. Guth, A.H. Inflationary universe: A possible solution to the horizon and flatness problems. *Phys. Rev. D* **1981**, *23*, 347–356. [CrossRef]
2. Starobinsky, A.A. Spectrum of relict gravitational radiation and the early state of the universe. *JETP Lett.* **1979**, *30*, 682–685.
3. Mukhanov, V.F.; Chibisov, G.V. Quantum Fluctuations and a Nonsingular Universe. *JETP Lett.* **1981**, *33*, 532–535.
4. Linde, A.D. Chaotic Inflation. *Phys. Lett. B* **1983**, *129*, 177–181. [CrossRef]
5. Hawking, S.W. The Development of Irregularities in a Single Bubble Inflationary Universe. *Phys. Lett. B* **1982**, *115*, 295. [CrossRef]
6. Hawking, S.W.; Moss, I.G. Fluctuations in the Inflationary Universe. *Nucl. Phys. B* **1983**, *224*, 180. [CrossRef]
7. Starobinsky, A.A. Dynamics of Phase Transition in the New Inflationary Universe Scenario and Generation of Perturbations. *Phys. Lett. B* **1982**, *117*, 175–178. [CrossRef]
8. Guth, A.H.; Pi, S.Y. Fluctuations in the New Inflationary Universe. *Phys. Rev. Lett.* **1982**, *49*, 1110–1113. [CrossRef]
9. Bardeen, J.M.; Steinhardt, P.J.; Turner, M.S. Spontaneous Creation of Almost Scale - Free Density Perturbations in an Inflationary Universe. *Phys. Rev. D* **1983**, *28*, 679. [CrossRef]
10. Giovannini, M. Spikes in the relic graviton background from quintessential inflation. *Class. Quant. Grav.* **1999**, *16*, 2905–2913. [CrossRef]
11. Giovannini, M. Production and detection of relic gravitons in quintessential inflationary models. *Phys. Rev. D* **1999**, *60*, 123511. [CrossRef]
12. Giovannini, M. Low scale quintessential inflation. *Phys. Rev. D* **2003**, *67*, 123512. [CrossRef]
13. Cognola, G.; Elizalde, E.; Nojiri, S.; Odintsov, S.D.; Sebastiani, L.; Zerbini, S. Class of viable modified $f(R)$ gravities describing inflation and the onset of accelerated expansion. *Phys. Rev. D* **2008**, *77*, 046009. [CrossRef]
14. Myrzakulov, R.; Sebastiani, L.; Vagnozzi, S. Inflation in $f(R, \phi)$ -theories and mimetic gravity scenario. *Eur. Phys. J. C* **2015**, *75*, 444. [CrossRef]
15. Salvio, A. Inflationary Perturbations in No-Scale Theories. *Eur. Phys. J. C* **2017**, *77*, 267. [CrossRef]
16. Salvio, A. Quasi-Conformal Models and the Early Universe. *Eur. Phys. J. C* **2019**, *79*, 750. [CrossRef]
17. Oikonomou, V.K. Viability of the intermediate inflation scenario with F(T) gravity. *Phys. Rev. D* **2017**, *95*, 084023. [CrossRef]
18. Agarwal, A.; Myrzakulov, R.; Sami, M.; Singh, N.K. Quintessential inflation in a thawing realization. *Phys. Lett. B* **2017**, *770*, 200–208. [CrossRef]
19. Keskin, A.I. Viable super inflation scenario from F(T) modified teleparallel gravity. *Eur. Phys. J. C* **2018**, *78*, 705. [CrossRef]
20. Castello, S.; Ilić, S.; Kunz, M. Updated dark energy view of inflation. *Phys. Rev. D* **2021**, *104*, 023522. [CrossRef]
21. Arkani–Hamed, N.; Dimopoulos, S.; Dvali, G. The hierarchy problem and new dimensions at a millimeter. *Phys. Lett. B* **1998**, *429*, 263–272. CrossRef]
22. Randall, L.; Sundrum, R. Large Mass Hierarchy from a Small Extra Dimension. *Phys. Rev. Lett.* **1999**, *83*, 3370–3373. [CrossRef]
23. Randall, L.; Sundrum, R. An Alternative to Compactification. *Phys. Rev. Lett.* **1999**, *83*, 4690–4693. [CrossRef]
24. Dvali, G.; Gabadadze, G.; Porrati, M. 4D gravity on a brane in 5D Minkowski space. *Phys. Lett. B* **2000**, *485*, 208–214. CrossRef]
25. Battye, R.A.; Carter, B. Generic junction conditions in brane-world scenarios. *Phys. Lett. B* **2001**, *509*, 331–336. CrossRef]
26. Maia, M.; Monte, E.M. Geometry of brane-worlds. *Phys. Lett. A* **2002**, *297*, 9–19. CrossRef]
27. Maia, M.D.; Monte, E.M.; Maia, J.M.F.; Alcaniz, J.S. On the geometry of dark energy. *Class. Quant. Grav.* **2005**, *22*, 1623. [CrossRef]
28. Maia, M.D.; Silva, N.; Fernandes, M.C.B. Brane-world quantum gravity. *J. High Energy Phys.* **2007**, *2007*, 47. [CrossRef]
29. Heydari-Fard, M.; Sepangi, H. Anisotropic brane gravity with a confining potential. *Phys. Lett. B* **2007**, *649*, 1–11. CrossRef]
30. Jalalzadeh, S.; Mehrnia, M.; Sepangi, H.R. Classical tests in brane gravity. *Class. Quant. Grav.* **2009**, *26*, 155007. [CrossRef]
31. Maia, M.D.; Capistrano, A.J.S.; Alcaniz, J.S.; Monte, E.M. The Deformable Universe. *Gen. Rel. Grav.* **2011**, *43*, 2685–2700. [CrossRef]
32. Ranjbar, A.; Sepangi, H.R.; Shahidi, S. Asymptotically Lifshitz Brane-World Black Holes. *Ann. Phys.* **2012**, *327*, 3170. [CrossRef]
33. Capistrano, A.J.S.; Cabral, L.A. Geometrical aspects on the dark matter problem. *Ann. Phys.* **2014**, *348*, 64–83. [CrossRef]
34. Capistrano, A.J.S.; Cabral, L.A. Implications on the cosmic coincidence by a dynamical extrinsic curvature. *Class. Quant. Grav.* **2016**, *33*, 245006. [CrossRef]

35. Capistrano, A.J.S. Constraints on cosmokinetics of smooth deformations. *Mon. Not. Roy. Astron. Soc.* **2015**, *448*, 1232–1239. [CrossRef]
36. Capistrano, A.J.S.; Gutiérrez-Piñeres, A.C.; Ulhoa, S.C.; Amorim, R.G. On classical thermal stability of black holes with a dynamical extrinsic curvature. *Ann. Phys.* **2017**, *380*, 106–120. [CrossRef]
37. Capistrano, A.J.S. Evolution of Density Parameters on a Smooth Embedded Universe. *Annalen der Physik.* **2018**, *530*, 1700232. [CrossRef]
38. Capistrano, A.J.S. Lukewarm black holes in the Nash-Greene framework. *Phys. Rev. D* **2019**, *100*, 064049. [CrossRef]
39. Capistrano, A.J.S.; Seidel, P.T.Z.; Duarte, H.R. Subhorizon linear Nash–Greene perturbations with constraints on H(z) and the deceleration parameter q(z). *Phys. Dark Univ.* **2021**, *31*, 100760. [CrossRef]
40. Capistrano, A.J.S.; Cabral, L.A.; Marão, J.A.P.F.; Coimbra-Araújo, C.H. Linear Nash-Greene fluctuations on the evolution of S8 and H0 tensions. *Eur. Phys. J.* **2022**, *82*, 1434–6052. [CrossRef]
41. Martin, J.; Ringeval, C.; Vennin, V. Encyclopædia Inflationaris. *Phys. Dark Univ.* **2014**, *5-6*, 75–235. [CrossRef]
42. Higson, E.; Handley, W.; Hobson, M.; Lasenby, A. Dynamic nested sampling: an improved algorithm for parameter estimation and evidence calculation. *Stat. Comput.* **2019**, *29*, 891–913. [CrossRef]
43. Speagle, J.S. dynesty: a dynamic nested sampling package for estimating Bayesian posteriors and evidences. *Mon. Not. Roy. Astron. Soc.* **2020**, *493*, 3132–3158. [CrossRef]
44. Chevallier, M.; Polarski, D. Accelerating universes with scaling dark matter. *Int. J. Mod. Phys. D* **2001**, *10*, 213–224. [CrossRef]
45. Linder, E.V. Exploring the expansion history of the universe. *Phys. Rev. Lett.* **2003**, *90*, 091301. [CrossRef]
46. Jr., E.M.B.; Alcaniz, J. Probing the time dependence of dark energy. *J. Cosmol. Astropart. Phys.* **2012**. *2012*, 42. [CrossRef]
47. Gupta, G.; Rangarajan, R.; Sen, A.A. Thawing quintessence from the inflationary epoch to today. *Phys. Rev. D* **2015**, *92*, 123003. [CrossRef]
48. Chiba, T. Slow-roll thawing quintessence. *Phys. Rev. D* **2009**, *79*, 083517. [CrossRef]
49. Scherrer, R.J.; Sen, A.A. Thawing quintessence with a nearly flat potential. *Phys. Rev. D* **2008**, *77*, 083515. [CrossRef]
50. Sahlen, M.; Liddle, A.R.; Parkinson, D. Quintessence reconstructed: New constraints and tracker viability. *Phys. Rev. D* **2007**, *75*, 023502. [CrossRef]
51. Schimd, C.; Tereno, I.; Uzan, J.P.; Mellier, Y.; van Waerbeke, L.; Semboloni, E.; Hoekstra, H.; Fu, L.; Riazuelo, A. Tracking quintessence by cosmic shear - constraints from virmos-descart and cfhtls and future prospects. *Astron. Astrophys.* **2007**, *463*, 405–421. :20065154 [CrossRef]
52. Chiba, T. w and $w^{'}$ of scalar field models of dark energy. *Phys. Rev. D* **2006**, *73*, 063501. [CrossRef]
53. Scherrer, R.J. Dark energy models in the w-w' plane. *Phys. Rev. D* **2006**, *73*, 043502. [CrossRef]
54. Eisenhart, L.P. *On Riemannian Geometry*; Dover Publications: New York, 2005.
55. Nash, J. C1 Isometric Imbeddings. *Ann. Math.* **1954**, *60*, 383–396. [CrossRef]
56. Nash, J. The Imbedding Problem for Riemannian Manifolds. *Ann. Math.* **1956**, *63*, 20–63. [CrossRef]
57. Greene, R.E. Isometric embeddings of Riemannian and pseudo-Riemannian manifolds. *Memoirs of the American Mathematical Society*; American Mathematical Society: Providence, RI, USA, 1970; Volume 63. [CrossRef]
58. Turner, M.S.; White, M.J. CDM models with a smooth component. *Phys. Rev. D* **1997**, *56*, R4439. [CrossRef]
59. Abbott, L.F.; Wise, M.B. Constraints on Generalized Inflationary Cosmologies. *Nucl. Phys. B* **1984**, *244*, 541–548. [CrossRef]
60. Lucchin, F.; Matarrese, S. Power Law Inflation. *Phys. Rev. D* **1985**, *32*, 1316. [CrossRef]
61. Davies, P.C.W.; Sahni, V. Quantum gravitational effects near cosmic strings. *Class. Quant. Grav.* **1988**, *5*, 1. [CrossRef]
62. Tristram, M.; Banday, A.J.; Górski, K.M.; Keskitalo, R.; Lawrence, C.R.; Andersen, K.J.; Barreiro, R.B.; Borrill, J.; Eriksen, H.K.; Fernandez-Cobos, R.; et al. Planck constraints on the tensor-to-scalar ratio. *Astron. Astrophys.* **2021**, *647*, A128. [CrossRef]
63. Becker, K.; Becker, M.; Krause, A. M-theory inflation from multi M5-brane dynamics. *Nucl. Phys. B* **2005**, *715*, 349–371. [CrossRef]
64. Bennai, M.; Chakir, H.; Sakhi, Z. On Inflation Potentials in Randall-Sundrum Braneworld Model. *Eur. J. Phys.* **2006**, *9*, 84–93.
65. Parsons, P.; Barrow, J.D. Generalized scalar field potentials and inflation. *Phys. Rev. D* **1995**, *51*, 6757–6763. [CrossRef] [PubMed]
66. Barrow, J.D.; Nunes, N.J. Dynamics of Logamediate Inflation. *Phys. Rev. D* **2007**, *76*, 043501. [CrossRef]
67. Clemson, T.G.; Liddle, A.R. Observational constraints on thawing quintessence models. *Mon. Not. Roy. Astron. Soc.* **2009**, *395*, 1585–1590. [CrossRef]
68. Pantazis, G.; Nesseris, S.; Perivolaropoulos, L. Comparison of thawing and freezing dark energy parametrizations. *Phys. Rev. D* **2016**, *93*, 103503. [CrossRef]
69. Foreman-Mackey, D.; Agol, E.; Ambikasaran, S.; Angus, R. Fast and Scalable Gaussian Process Modeling with Applications to Astronomical Time Series. *Astron. J.* **2017**, *154*, 220. [CrossRef]
70. Jeffreys, H. *Theory of Probability*, 3rd ed.; Oxford University Press: Oxford, UK, 1961.